THE JOURNAL OF BIOLOGICAL CHEMISTRY VOL. 283, NO. 34, pp. 23217–23223, August 22, 2008
© 2008 by The American Society for Biochemistry and Molecular Biology, Inc. Printed in the U.S.A.

The α_{1S} III-IV Loop Influences 1,4-Dihydropyridine Receptor Gating but Is Not Directly Involved in Excitation-Contraction Coupling Interactions with the Type 1 Ryanodine Receptor*

Received for publication, June 4, 2008, and in revised form, June 13, 2008 Published, JBC Papers in Press, June 13, 2008, DOI 10.1074/jbc.M804312200

Roger A. Bannister[‡1], **Manfred Grabner**[§], **and Kurt G. Beam**[‡2]

From the [‡]*Department of Physiology and Biophysics, University of Colorado-Denver, Aurora, Colorado 80045 and the* [§]*Department of Medical Genetics, Clinical and Molecular Pharmacology, Innsbruck Medical University, A-6020 Innsbruck, Austria*

In skeletal muscle, coupling between the 1,4-dihydropyridine receptor (DHPR) and the type 1 ryanodine receptor (RyR1) underlies excitation-contraction (EC) coupling. The III-IV loop of the DHPR α_{1S} subunit binds to a segment of RyR1 *in vitro*, and mutations in the III-IV loop alter the voltage dependence of EC coupling, raising the possibility that this loop is directly involved in signal transmission from the DHPR to RyR1. To clarify the role of the α_{1S} III-IV loop in EC coupling, we examined the functional properties of a chimera (GFP-α_{1S}[III-IVa]) in which the III-IV loop of the divergent α_{1A} isoform replaced that of α_{1S}. *Dysgenic* myotubes expressing GFP-α_{1S}[III-IVa] yielded myoplasmic Ca^{2+} transients that activated at ~10 mV more hyperpolarized potentials and that were ~65% smaller than those of GFP-α_{1S}. A similar reduction was observed in voltage-dependent charge movements for GFP-α_{1S}[III-IVa], indicating that the chimeric channels trafficked less well to the membrane but that those that were in the membrane functioned as efficiently in EC coupling as GFP-α_{1S}. Relative to GFP-α_{1S}, L-type currents mediated by GFP-α_{1S}[III-IVa] were ~40% smaller and activated at ~5 mV more hyperpolarized potentials. The altered gating of GFP-α_{1S}[III-IVa] was accentuated by exposure to ±Bay K 8644, which caused a much larger hyperpolarizing shift in activation compared with its effect on GFP-α_{1S}. Taken together, our observations indicate that the α_{1S} III-IV loop is not directly involved in EC coupling but does influence DHPR gating transitions important both for EC coupling and activation of L-type conductance.

The skeletal muscle L-type Ca^{2+} channel (1,4-dihydropyridine receptor; DHPR)[3] serves as the voltage sensor for excitation-contraction (EC) coupling, activating Ca^{2+} release from the sarcoplasmic reticulum via the type 1 ryanodine receptor (RyR1) in response to depolarization of the plasma membrane (1). Skeletal muscle DHPRs are heteromultimeric channels composed of a primary α_{1S} subunit and auxiliary β_{1a}, $\alpha_2\delta$-1, and γ_1 subunits (2). Neither genetic ablation of DHPR γ_1 subunits (3, 4) nor small interfering RNA knockdown of DHPR $\alpha_2\delta$-1 subunits (5–7) seem to have pronounced effects on coupling of the DHPR with RyR1. On the other hand, the DHPR α_{1S} and β_1 subunits are essential for EC coupling (8, 9). Mice null for either the α_{1S} or β_1 subunit die perinatally because of respiratory paralysis. EC coupling can be restored in myotubes cultured from the respective null mouse pups, as well as from β_1 null zebrafish embryos, by heterologous expression of the missing subunit (1, 9–17).

The inability of heterologously expressed cardiac (α_{1C}) DHPRs to restore skeletal-type (*i.e.* Ca^{2+} entry-independent) EC coupling in *dysgenic* (α_{1S} null) myotubes (18, 19) enabled Tanabe *et al.* (10) to employ chimeric DHPRs as a means to probe regions of α_{1S} that are essential for skeletal-type EC coupling. In that study, the chimera containing the α_{1S} II-III loop was the only chimera with a single loop substitution that was capable of restoring EC coupling similar to that observed for wild-type α_{1S} when expressed in *dysgenic* myotubes. Subsequently, the experimental approach of expressing progressively more complex α_{1S}/α_{1C} chimeras in *dysgenic* myotubes identified a subdomain within the α_{1S} II-III loop (residues 720–765, the "critical domain") that was necessary to support skeletal-type EC coupling ("orthograde coupling") (20–22). Similarly, the critical domain also has been found to be a major determinant for RyR1-dependent enhancement of the L-type current ("retrograde coupling") (23).

Although an essential role for the critical domain in skeletal EC coupling has been established (Refs. 20–22, 24, and 25; but see Ref. 26), roles for other intracellular loops of the α_{1S} subunit have also been proposed (27). For example, the α_{1S} carboxyl terminus facilitates expression and targeting of the DHPR (28, 29), most likely by interacting with other junctional proteins (*e.g.* RyR1) (30–34). The α_{1S} I-II loop is essential for EC coupling because it is the site of interaction with β_{1a} (35–37). The α_{1S} amino terminus does not play a major role in EC coupling, because deletion of the bulk of the amino terminus has little effect on EC coupling (38).

In contrast to the relatively well defined roles of the other intracellular regions of α_{1S} in EC coupling, little is known about the contribution of the α_{1S} III-IV loop. A potentially important

* This work was supported, in whole or in part, by National Institutes of Health Grants NS24444 and AR44750 (to K. G. B.). This work was also supported by Fonds zur Förderung der wissenschaftlichen Forschung Grant P16098-B04 (to M. G.). The costs of publication of this article were defrayed in part by the payment of page charges. This article must therefore be hereby marked "*advertisement*" in accordance with 18 U.S.C. Section 1734 solely to indicate this fact.

[1] Supported by Muscular Dystrophy Association Developmental Grant MDA4155.

[2] To whom correspondence should be addressed: Dept. of Physiology and Biophysics, University of Colorado-Denver, P.O. Box 6511, Mail Stop F8307, Aurora, CO 80045. Tel.: 303-724-4542; Fax: 303-724-4501; E-mail: kurt.beam@uchsc.edu.

[3] The abbreviations used are: DHPR, 1,4-dihydropyridine receptor; EC, excitation-contraction; RyR1, type 1 ryanodine-sensitive intracellular Ca^{2+} release channel; GFP, green fluorescent protein.

role for the α_{1S} III-IV loop in EC coupling was first raised by its identification as the locus for the only DHPR mutations (R1086H and R1086C) currently linked to malignant hyperthermia (39). Functional analysis of the R1086H mutant channel expressed in a *dysgenic* cell line showed that the α_{1S} R1086H mutation causes a hyperpolarizing shift in the activation of myoplasmic Ca^{2+} transients (40). In addition, the α_{1S} III-IV loop has also been identified as a potential site of DHPR-RyR1 protein-protein interaction by virtue of the ability of an α_{1S} III-IV loop-glutathione *S*-transferase fusion protein to bind a purified fragment of RyR1 (residues 922–1112) *in vitro* (41).

Previous studies seeking to identify α_{1S} cytoplasmic domains important for EC coupling have made use of chimeras of α_{1S} and α_{1C} (10, 42). Although these studies have been invaluable, they have not been revealing about the III-IV loop because it is highly conserved between α_{1S} and α_{1C} (46/53 residues conserved). To test the contribution of the α_{1S} III-IV loop to EC coupling more stringently, we examined the functional characteristics of an α_{1S}-based chimera that incorporated the relatively nonconserved (29 of 53 residues) III-IV loop of the neuronal P/Q-type channel α_{1A} in place of the α_{1S} III-IV loop. Our results indicate that the α_{1S} III-IV loop influences conformational transitions of the DHPR, including transitions important for EC coupling. However, it is unlikely to represent a DHPR-RyR1 site of contact that is necessary for EC coupling.

EXPERIMENTAL PROCEDURES

Myotube Culture and Expression of cDNA—All of the procedures involving mice were approved by the University of Colorado-Denver Institutional Animal Care and Use Committee. Primary cultures of *dysgenic* myotubes were prepared from newborn mice as described previously (43). For electrophysiological experiments, myoblasts were plated on 35-mm ECL-coated, plastic culture dishes (number 353801; Falcon, San Jose, CA). Cultures were grown for 6–7 days in a humidified 37 °C incubator with 5% CO_2 in Dulbecco's modified Eagle's medium (number 15-017-CM; Mediatech, Herndon, VA), supplemented with 10% fetal bovine serum/10% horse serum (Hyclone Laboratories, Logan, UT). This medium was then replaced with differentiation medium (Dulbecco's modified Eagle's medium supplemented with 2% horse serum). Two to four days after the switch to differentiation medium, single nuclei were microinjected with cDNA (400 ng/μl) encoding either GFP-α_{1S} or GFP-α_{1S}[III-IVa]. GFP-α_{1S} (GenBank™ accession number X05921) and GFP-α_{1S}[III-IVa] were constructed as previously described (44, 29).

Measurement of Ionic Currents—Myotubes were used in electrophysiological experiments 2 days following injection. Pipettes were fabricated from borosilicate glass and had resistances of ~1.5 MΩ when filled with internal solution, which consisted of 140 mM cesium aspartate, 10 mM Cs_2-EGTA, 5 mM $MgCl_2$, and 10 mM HEPES, pH 7.4, with CsOH. The external solution contained 145 mM tetraethylammonium chloride, 10 mM $CaCl_2$, 0.003 mM tetrodotoxin, and 10 mM HEPES, pH 7.4, with tetraethylammonium-OH. In some experiments, L-type currents were recorded in the continuous presence of racemic Bay K 8644 (10 μM; kindly supplied by Dr. A. Scriabine, Miles Laboratories Inc., New Haven, CT) in the bath solution. Linear capacitative and leakage currents were determined by averaging the currents elicited by eleven 30-mV hyperpolarizing pulses from a holding potential of −80 mV. Test currents were corrected for linear components of leak and capacitive current by digital scaling and subtraction of this average control current. Electronic compensation was used to reduce the effective series resistance (usually to <1 MΩ) and the time constant for charging the linear cell capacitance (usually to <0.5 ms). Ionic currents were filtered at 2 kHz (eight pole Bessel filter; Frequency Devices, Inc.) and digitized at 10 kHz. To measure macroscopic L-type current in isolation, a 1-s prepulse to −20 mV followed by a 50-ms repolarization to −50 mV was administered before the test pulse (prepulse protocol) (11) to inactivate T-type Ca^{2+} channels. Cell capacitance was determined by integration of a transient from −80 mV to −70 mV using Clampex 8.0 (Axon Instrument, Foster City, CA) and was used to normalize current amplitudes (pA/pF). Current-voltage (*I-V*) curves were fitted using the following Boltzmann expression,

$$I = G_{max}*(V - V_{rev})/\{1 + \exp[-(V - V_{1/2})/k_G]\} \quad \text{(Eq. 1)}$$

where I is the current for the test potential V, V_{rev} is the reversal potential, G_{max} is the maximum Ca^{2+} channel conductance, $V_{½}$ is the half-maximal activation potential, and k_G is the slope factor. Tail-current amplitude (I_{tail}) was measured 1 ms after the onset of the repolarization from the test pulse to −50 mV (45).

Measurement of Intracellular Ca^{2+} Transients—Changes in intracellular Ca^{2+} were recorded with Fluo-3 (F-3715; Molecular Probes, Eugene, OR) in the whole cell configuration. The salt form of the dye was added to the standard internal solution for a final concentration of 200 nM. After entry into the whole cell configuration, a waiting period of >5 min was used to allow the dye to diffuse into the cell interior. A 100-W mercury illuminator and a set of fluorescein filters were used to excite the dye present in a small rectangular region of the voltage-clamped myotube. A computer-controlled shutter was used to block illumination in the intervals between test pulses. Fluorescence emission was measured by means of a fluorometer apparatus (Biomedical Instrumentation Group, University of Pennsylvania, Philadelphia, PA). The average background fluorescence was quantified before bath immersion of the patch pipette. Fluorescence data are expressed as $\Delta F/F$, where ΔF represents the change in peak fluorescence from base line during the test pulse, and F is the fluorescence immediately prior to the test pulse minus the average background (non-Fluo-3) fluorescence. Unless otherwise noted, the peak value of the fluorescence change ($\Delta F/F$) for each test potential (V) was fitted according to the following equation,

$$(\Delta F/F) = (\Delta F/F)_{max}/\{1 + \exp[(V_F - V)/k_F]\} \quad \text{(Eq. 2)}$$

where $(\Delta F/F)_{max}$ is the maximal fluorescence change, V_F is the potential causing half the maximal change in fluorescence, and k_F is a slope parameter.

Electrically Evoked Contractions—Contractions were elicited by 20-ms, 100-V stimuli applied via an extracellular pipette that contained 150 mM NaCl and was placed near intact myotubes expressing constructs of interest. The myotubes

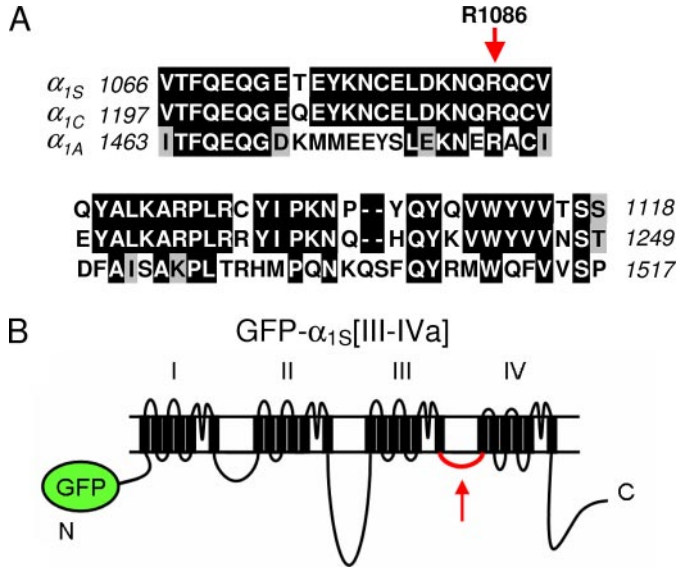

FIGURE 1. **Rationale for examination of the functional properties of the GFP-α_{1S}[III-IVa] chimera.** *A*, sequence comparison of the III-IV loops of rabbit α_{1S} (GenBank™ accession number X05921), rabbit α_{1C} (GenBank™ accession number X15539), and rabbit α_{1A} (GenBank™ accession number X57477). Residues of α_{1C} or α_{1A} identical to those of α_{1S} are shown *boxed* in *black*, and residues conserved with those of α_{1S} are shown *boxed* in *gray*. Note that the residue corresponding to α_{1S} R1086 (indicated with a *red arrow*) that, if exchanged to H or C is linked to the MH phenotype, is conserved in all three channels. *B*, schematic representation of GFP-α_{1S}[III-IVa].

were bathed in rodent Ringer's solution (146 mM NaCl, 5 mM KCl, 2 mM $CaCl_2$, 1 mM $MgCl_2$, 10 mM HEPES, 11 mM glucose, pH 7.4, with NaOH). Contractions were assayed by the movement of an identifiable portion of a myotube across the visual field.

Measurement of Charge Movements—For recordings of immobilization-resistant intramembrane charge movements as a measure of functional DHPR channel expression, ionic currents were blocked by the addition of 0.5 mM $CdCl_2$ + 0.1 mM $LaCl_3$ to the standard extracellular recording solution. All of the charge movements were corrected for linear cell capacitance and leakage currents using a −P/8 subtraction protocol (46). Filtering was at 2 kHz, and digitization was at 20 kHz. Voltage clamp command pulses were exponentially rounded with a time constant of 50–500 μs, and the prepulse protocol (see above) was used to reduce the contribution of gating currents from voltage-gated Na^+ channels and T-type Ca^{2+} channels. The integral of the depolarization transient (Q_{on}) for each test potential (V) was fitted according to the following equation,

$$Q_{on} = Q_{max}/\{1 + \exp[(V_Q - V)/k_Q]\} \quad \text{(Eq. 3)}$$

where Q_{max} is the maximal Q_{on}, V_Q is the potential causing movement of half the maximal charge, and k_Q is a slope parameter.

Analysis—The figures were made using the software program SigmaPlot (version 7.0, Systat Software, Inc., San Jose, CA). All of the data are presented as the means ± S.E. Statistical comparisons were by unpaired, two-tailed t test (as appropriate), with $p < 0.05$ considered significant.

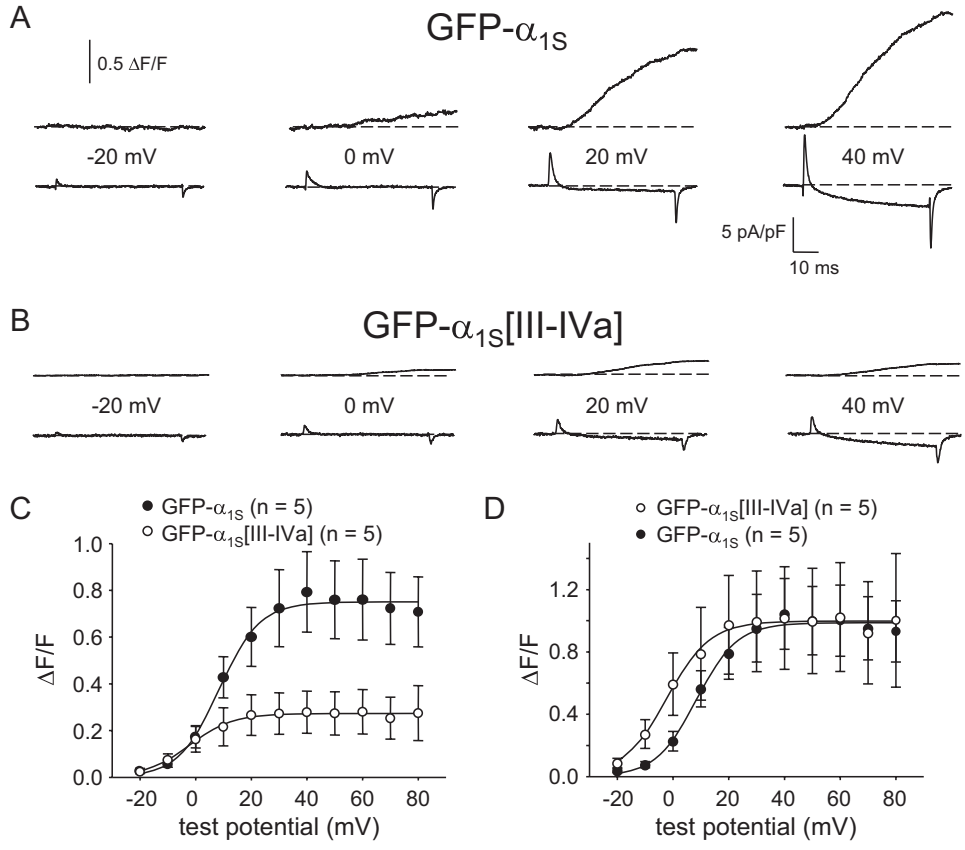

FIGURE 2. **EC coupling is reduced in myotubes expressing GFP-α_{1S}[III-IVa].** Simultaneous recordings of myoplasmic Ca^{2+} transients (*top*) and L-type Ca^{2+} currents (*bottom*), elicited by 50-ms depolarizations from −50 mV to the indicated test potentials are shown for *dysgenic* myotubes expressing either GFP-α_{1S} (*A*) or GFP-α_{1S}[III-IVa] (*B*). *C*, average Δ*F*/*F*-*V* relationships. *D*, Δ*F*/*F*-*V* relationships normalized to average Δ*F*/*F* at +50 mV to allow direct comparison of voltage dependence. The *smooth curves* are plotted according to Equation 2, with fit parameters presented in Table 1. Throughout, the *error bars* represent ± S.E.

RESULTS

The primary experimental approach that has been used to determine the contributions of the α_{1S} cytoplasmic domains to skeletal-type EC coupling is to characterize Ca^{2+} transients produced by chimeras of α_{1S} and α_{1C} (10, 20, 42). However, this approach is of limited value for the III-IV loop because it is highly conserved between α_{1S} and α_{1C} (Fig. 1*A*). In the present study, we examined the functional characteristics of a chimera in which the less conserved III-IV loop of the α_{1A} subunit of the neuronal high voltage-activated P/Q type channel was incorporated into the corresponding region of α_{1S} (chimera GFP-α_{1S}[III-IVa]; Fig. 1*B*).

Ca^{2+} Release Is Reduced in Myotubes Expressing GFP-α_{1S}[III-IVa]—Myoplasmic Ca^{2+} transients were measured in the whole cell patch clamp configuration to deter-

TABLE 1

$\Delta F/F - V$ parameters and electrically-evoked contractions

The parameters for $\Delta F/F - V$ were obtained by best fits of the raw data according to Equation 2. The values are given as the means ± S.E., with the number of myotubes tested indicated in parentheses. *ND*, not determined.

Construct	$\Delta F/F - V$			Contracting cells/tested
	$\Delta F/F_{max}$	V_F	k_F	
	ΔF/F	*mV*	*mV*	
GFP-α_{1S}	0.75 ± 0.16 (5)	8.1 ± 2.1	7.1 ± 2.1	22/39[c]
GFP-α_{1S}[III-IVa]	0.27 ± 0.09 (5)[a]	−2.0 ± 1.9[b]	8.1 ± 1.1	10/16
Uninjected *dysgenic* myotubes		ND		0/91

[a] Significant difference from GFP-α_{1S} ($p < 0.05$).
[b] Significant difference from GFP-α_{1S} ($p < 0.01$).
[c] Data from Ref. 24.

mine whether replacement of the α_{1S} III-IV loop by that of α_{1A} affects EC coupling. As shown in Fig. 2*A*, GFP-α_{1S} expressing *dysgenic* myotubes produced robust Ca^{2+} transients with an average $\Delta F/F_{max}$ of 0.75 ± 0.16 $\Delta F/F$ ($n = 5$). In contrast, *dysgenic* myotubes expressing GFP-α_{1S}[III-IVa] yielded Ca^{2+} transients that were considerably smaller in magnitude ($\Delta F/F_{max}$ = 0.27 ± 0.09; $n = 5$; $p < 0.05$; Fig. 2*B*). The reduction in $\Delta F/F_{max}$ observed for GFP-α_{1S}[III-IVa] was accompanied by a substantial (~10 mV; $p < 0.01$) hyperpolarizing shift in voltage dependence of Ca^{2+} release (Fig. 2*C* and Table 1). This shift became more apparent when the respective $\Delta F/F$-*V* curves were normalized to the average $\Delta F/F$ measured at +50 mV (Fig. 2*D*). Although the magnitude of Ca^{2+} release in response to depolarization from the sarcoplasmic reticulum was reduced in comparison with GFP-α_{1S}, GFP-α_{1S}[III-IVa] was still capable of producing myotube contractions evoked by extracellular electrical stimulation (10 of 16 myotubes tested; Table 1).

L-type Ca^{2+} Currents Are Reduced in Myotubes Expressing GFP-α_{1S}[III-IVa]—As expected, GFP-α_{1S} produced large, slowly activating L-type currents (-4.7 ± 0.6 pA/pF at +40 mV; $n = 13$; Fig. 3*A*, *left panel*) when expressed in *dysgenic* myotubes. By comparison, L-type currents were smaller in *dysgenic* myotubes expressing GFP-α_{1S}[III-IVa] (-3.1 ± 0.3 pA/pF; $n = 20$; $p < 0.05$; Fig. 3*A*, *right panel*). Based on fitting with Equation 1, there was also a hyperpolarizing shift in the voltage dependence of activation for GFP-α_{1S}[III-IVa] in comparison with GFP-α_{1S} ($V_{½}$ = 28.9 ± 1.0 mV *versus* 32.5 ± 1.5 mV, respectively; $p < 0.05$; Fig. 3*B* and Table 2). Based on this same analysis with Equation 1, the reduction in G_{max} was ~25%. It should be noted that the reversal potential for GFP-α_{1S}[III-IVa] was routinely shifted by ~10 mV to more hyperpolarized potentials (Fig. 3*B*). Such a shift in reversal potential is typical of low magnitude L-type currents recorded under similar conditions (47–50), which most likely occurs because of contamination by outward currents. Thus, we also used tail currents (I_{tail}) to estimate relative conductances because these are unaffected by changes in apparent reversal potential (Fig. 3*C*). Tail currents at −50 mV upon repolarization from +40 mV ("$I_{tail}(40)$") were −11.2 ± 1.8 pA/pF in *dysgenic* myotubes expressing GFP-α_{1S} ($n = 13$) and −6.3 ± 0.8 pA/pF in *dysgenic* myotubes expressing GFP-α_{1S}[III-IVa] ($n = 11$; $p < 0.05$).

Charge Movements Are Reduced in Myotubes Expressing GFP-α_{1S}[III-IVa]—Immobilization-resistant charge movements in GFP-α_{1S}[III-IVa] expressing myotubes were reduced by 65% relative to GFP-α_{1S}-expressing myotubes (Q_{max} = 2.9 ± 0.5 nC/μF; $n = 5$ *versus* 8.3 ± 1.3 nC/μF; $n = 6$, respectively; $p = 0.0051$; Fig. 4, *A* and *B*). A small hyperpolarizing shift was also observed for GFP-α_{1S}[III-IVa], but this shift was not significant (Table 2). Importantly, the reduction in Q_{max} (Fig. 4*B* and Table 2) was nearly equal in magnitude to the reduction in maximal Ca^{2+} transients for GFP-α_{1S}[III-IVa] (Fig. 2*C* and Table 1). Thus, GFP-α_{1S}[III-IVa] appeared to have an ability to activate Ca^{2+} release via RyR1 that was similar to that of GFP-α_{1S} (Fig. 4*C*, *left panel*). However, the reduction in peak Ca^{2+} current for GFP-α_{1S}[III-IVa] (Fig. 3*B*) was smaller than the reduction in Q_{max}, suggesting that P_o is higher for the chimeric channels. To assess the change in P_o more directly, we calculated the ratio between $I_{tail}(40)$ and Q', where Q' is the measured, maximal charge (Q_{max}) corrected for the charge that is present in uninjected *dysgenic* myotubes ($Q_{dys;}$ 0.9 ± 0.2 nC/μF; $n = 3$). This ratio provides an indication of channel P_o (11, 51). The ratio $I_{tail}(40)/Q'$ was substantially larger for GFP-α_{1S}[III-IVa] than for GFP-α_{1S} (3.2 *versus* 1.5 pA/fC, respectively; Fig. 4*C*, *right panel*, and Table 2).

GFP-α_{1S}[III-IVa] Is Potentiated by ±Bay K 8644—We wondered whether the elevated P_o for GFP-α_{1S}[III-IVa] would affect the response of the chimeric channel to the L-type Ca^{2+} channel agonist Bay K 8644, because this agent is also known to increase the P_o of L-type channels. In agreement with previous work on native skeletal muscle L-type channels (52), applica-

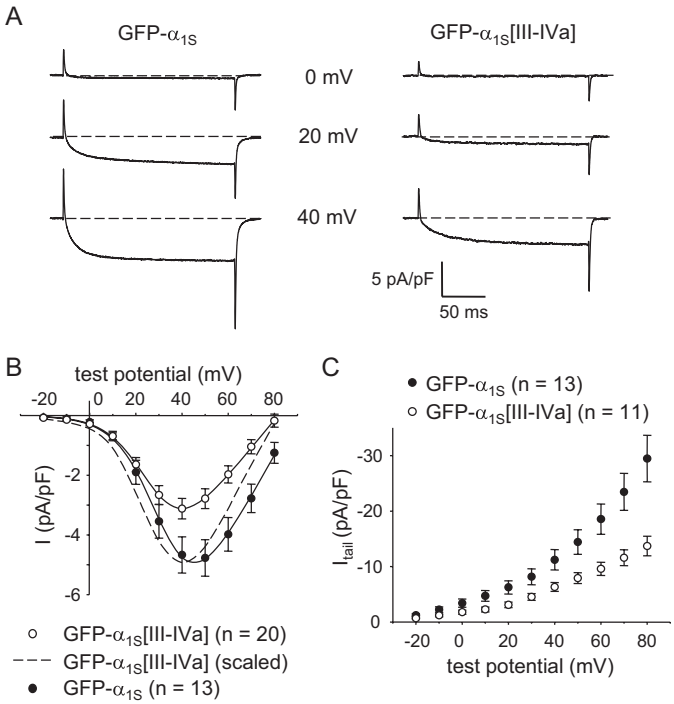

FIGURE 3. **L-type Ca^{2+} currents are reduced in myotubes expressing GFP-α_{1S}[III-IVa].** *A*, recordings of L-type Ca^{2+} currents, elicited by 200-ms depolarizations to the indicated test potentials are shown for *dysgenic* myotubes expressing GFP-α_{1S} or GFP-α_{1S}[III-IVa]. *B*, comparison of average peak *I-V* relationships. The dashed curve represents the *I-V* relationship for GFP-α_{1S}[III-IVa] scaled to match the peak current density for GFP-α_{1S}. The currents were evoked at 0.1 Hz by test potentials ranging from −20 mV through +80 mV in 10-mV increments following a prepulse protocol (11). The current amplitudes were normalized by linear cell capacitance (pA/pF). The smooth *I-V* curves are plotted according to Equation 1. The best fit parameters for each plot are presented in Table 2. *C*, tail current amplitudes measured 1 ms after repolarization to −50 mV are plotted as a function of the preceding test potential.

TABLE 2

Conductance and intramembrane charge movement

The best fit parameters determined by fitting peak I-V data according to Equation 1 and *Q-V* data according to Equation 3. The values are given as the means ± S.E. with the number of myotubes tested given in parentheses. $I_{tail}(40)$ represents the average amplitude of the current measured 1 ms after repolarizing to −50 mV after a 200-ms depolarization to +40 mV. $Q' = Q_{max} - Q_{dys}$, using the average values for each given in the table. ND, not determined. For all of the data given, the calculated average voltage error was <5 mV.

Construct	*G-V*			*Q-V*			
	G_{max}	$V_{½}$	k_G	Q_{max}	V_Q	k_Q	$I_{tail}(40)/Q$
	nS/nF	*mV*	*mV*	*nC/microfarad*	*mV*	*mV*	*pA/fC*
GFP-α_{1S}	128 ± 10 (13)	32.5 ± 1.5	8.1 ± 0.4	8.3 ± 1.3 (6)	−0.6 ± 3.0	13.5 ± 1.7	1.5
GFP-α_{1S}[III-IVa]	96 ± 8 (20)[a]	28.9 ± 1.0[a]	8.4 ± 0.3	2.9 ± 0.5 (5)[b]	−5.2 ± 3.7	10.6 ± 2.6	3.2
GFP-α_{1S} + Bay K 8644	181 ± 24 (8)[a]	29.2 ± 2.3	6.9 ± 0.3[a]		ND		ND
GFP-α_{1S}[III-IVa] + Bay K 8644	148 ± 16 (7)	19.9 ± 2.6[b]	6.7 ± 0.9		ND		ND
Uninjected *dysgenic* myotubes		No inward current (13)		0.9 ± 0.2 (3)[b]	−22.8 ± 3.5[b]	3.4 ± 2.9[b]	ND

[a] Significant difference from GFP-α_{1S} ($p < 0.05$).
[b] Significant difference from GFP-α_{1S} ($p < 0.01$).

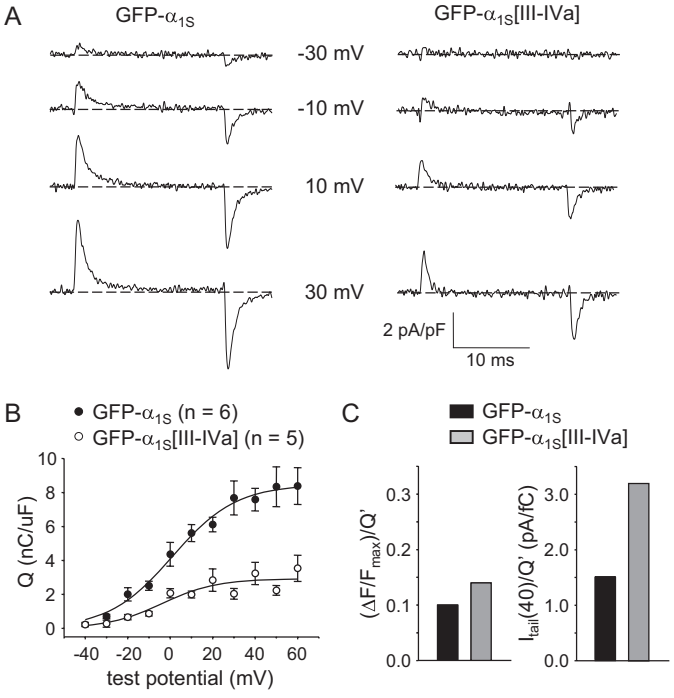

FIGURE 4. **GFP-α_{1S}[III-IVa] releases Ca^{2+} as efficiently as GFP-α_{1S} but has a higher L-type channel open probability (P_o).** *A*, recordings of immobilization-resistant charge movements elicited by 20-ms depolarizations from −50 mV to the indicated test potentials are shown for *dysgenic* myotubes expressing GFP-α_{1S} or GFP-α_{1S}[III-IVa]. *B*, comparison of Q-V relationships. Charge movements were evoked at 0.1 Hz by test potentials ranging from −40 mV through +60 mV in 10-mV increments, following a prepulse protocol (11). The *smooth curves* are plotted according to Equation 3, with best fit parameters presented in Table 2. *C*, $(\Delta F/F)_{max}/Q'$ and $I_{tail}(40)/Q'$ (*left* and *right*, respectively) for GFP-α_{1S} and GFP-α_{1S}[III-IVa]. Q' represents the charge attributable to heterologously expressed DHPRs in the membrane and was calculated as $Q_{max} - Q_{dys}$ (Table 2). The values for $(\Delta F/F)_{max}$ are from Table 1. The values for $I_{tail}(40)$ are given in the text and Table 2.

tion of ±Bay K 8644 (10 μM) caused an increase in peak current for GFP-α_{1S} (Fig. 5*A*) that was relatively modest compared with the effect on native α_{1C} (53, 54). The most prominent effect was a slowing of tail current decay (Fig. 5*A*, *inset*), which was also seen for GFP-α_{1S}[III-IVa] (Fig. 5*B*, *inset*). However, GFP-α_{1S}[III-IVa] differed from GFP-α_{1S} in that ±Bay K 8644 caused a pronounced leftward shift in activation (Fig. 5*B* and Table 2). This shift meant that the potentiation of peak current by ±Bay K 8644 was much greater for GFP-α_{1S}[III-IVa] than for GFP-α_{1S} at less depolarized potentials (Fig. 5*C*). The differential effect of ±Bay K 8644 is another indication that the III-IV loop influences gating transitions of the DHPR.

DISCUSSION

In the current study, depolarization-triggered myoplasmic Ca^{2+} transients in *dysgenic* myotubes expressing GFP-α_{1S}[III-IVa] were found to be activated ~10 mV more negatively and to be reduced by ~65% in amplitude, compared with those of GFP-α_{1S} (Fig. 2 and Table 1). L-type Ca^{2+} currents were also reduced for GFP-α_{1S}[III-IVa], but to a lesser extent (~40%) than the Ca^{2+} transients, and were also shifted to more hyperpolarizing potentials (Fig. 3). Immobilization-resistant charge movements were reduced by ~65% for GFP-α_{1S}[III-IVa] (Fig. 4 and Table 2), similar to the reduction in the magnitude of Ca^{2+} transients but larger than the reduction in L-type Ca^{2+} currents. Calculation of the ratio between tail current amplitude ($I_{tail}(40)$) and the charge attributable to DHPRs inserted into the membrane following construct cDNA injection (Q') indicated that channel P_o was increased about 2-fold for GFP-α_{1S}[III-IVa] compared with GFP-α_{1S} (Fig. 4). The hyperpolarizing shift in GFP-α_{1S}[III-IVa] channel activation was accentuated by exposure to the L-type channel agonist ±Bay K 8644 (Fig. 5).

The observation of a hyperpolarizing shift in Ca^{2+} release for GFP-α_{1S}[III-IVa] compared with GFP-α_{1S} (Fig. 2 and Table 1) supports the idea that the α_{1S} III-IV loop is in some way involved in EC coupling. Such an involvement was proposed by Weiss *et al.* (40) on the basis of a similar hyperpolarizing shift for an α_{1S} construct containing the R1086H point mutation, which is located in the III-IV loop and has been linked to the malignant hyperthermia phenotype. One possibility for the involvement of the α_{1S} III-IV loop in controlling sarcoplasmic reticulum Ca^{2+} release would be by direct interaction with RyR1, as suggested by the *in vitro* binding of this loop to a fragment (residues 922–1112) of RyR1 (41). If such a direct interaction were important, one might predict that the efficiency of EC coupling would be reduced for GFP-α_{1S}[III-IVa] because the sequence of its III-IV loop differs significantly from that of wild-type α_{1S} (Fig. 1). As an indicator of this efficiency, we calculated the ratio of $\Delta F/F_{max}$ (the maximum change in Fluo-3 fluorescence elicited by a 50-ms depolarization) to Q' (which equals $Q_{max} - Q_{dys}$ and is the charge attributable to recombinant DHPRs in the plasma membrane) (11). Because

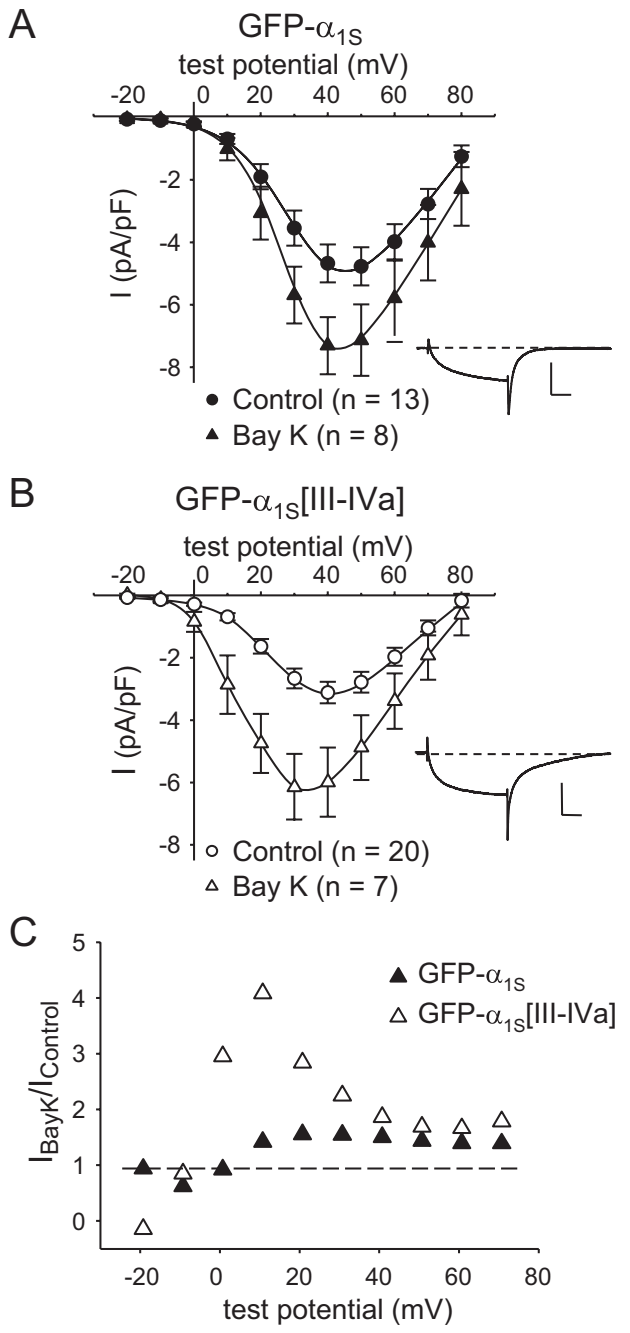

FIGURE 5. **GFP-α_{1S}[III-IVa] is more sensitive to ±Bay K 8644 than GFP-α_{1S}.** *A*, average peak *I-V* relationships for GFP-α_{1S} in the presence (▲, $n = 8$) and absence (●, $n = 13$) of 10 μM ±Bay K 8644. *B*, average peak *I-V* relationships for GFP-α_{1S}[III-IVa] in the presence (△, $n = 7$) and absence (○, $n = 20$) of 10 μM ±Bay K 8644. In both (*A*) and (*B*), peak *I-V* data obtained in the absence of ±Bay K 8644 are replotted from Fig. 3, and the *smooth curves* are plotted according to Equation 1 with best fit parameters given in Table 2. The *insets* illustrate representative currents obtained at a test potential of +30 mV in the presence of ±Bay K 8644. The *vertical scale bar* equals 5 pA/pF. The *horizontal scale bar* equals 50 ms. Note that these tail currents decay more slowly than currents in the absence of ±Bay K 8644 (Fig. 3*A*). *C*, potentiation ratios ($I_{Bay\ K\ 8644}/I_{untreated}$) for GFP-$\alpha_{1S}$ (▲) or GFP-α_{1S}[III-IVa] (△). The *dashed line* represents a potentiation ratio of 1.

the value of $(\Delta F/F_{max})/Q'$ was very similar for GFP-α_{1S}[III-IVa] and GFP-α_{1S} (Fig. 4*C*), it seems unlikely that an interaction between the α_{1S} III-IV loop and RyR1 plays an important role in EC coupling. Furthermore, the fraction of cells contracting in response to focal extracellular stimulation was similar for cells expressing GFP-α_{1S}[III-IVa] and GFP-α_{1S} (Table 1). This result supports the idea that the reduced number of GFP-α_{1S}[III-IVa] channels in the plasma membrane were effectively targeted to junctions with RyR1 (29) and elicited local Ca^{2+} release fluxes comparable with those elicited by GFP-α_{1S}.

Although our data provide evidence against a direct interaction of the α_{1S} III-IV loop with RyR1, they are consistent with the hypothesis that this loop is important for regulating gating transitions of other regions of the DHPR that are coupled directly to activation of RyR1. In particular, we observed that three features of L-type Ca^{2+} current were significantly altered for GFP-α_{1S}[III-IVa]: 1) activation was shifted in the hyperpolarizing direction, 2) P_o was increased, and 3) sensitivity to potentiation by ±Bay K 8644 was enhanced. Each of these effects indicate that substitution of the α_{1A} III-IV loop for that of α_{1S} promotes transitions of the channel from closed states into open states, which can be accounted for by the hypothesis that the wild-type α_{1S} III-IV loop stabilizes resting states of the DHPR. Because some of the gating transitions of the DHPR that result in activation of L-type current may also be involved in activation of RyR1, it seems reasonable that the α_{1S} III-IV loop might also inhibit depolarization-induced DHPR conformational changes that activate RyR1. This hypothesis would account for the hyperpolarizing shift in Ca^{2+} release observed for GFP-α_{1S}[III-IVa] if substitution of the α_{1A} III-IV loop removed the inhibitory effect of the wild-type α_{1S} III-IV loop on depolarization-induced DHPR conformational changes.

The maximal P_o is typically very low (<0.1) for L-type channels containing either α_{1S} (55) or α_{1C} (56) as the principle subunit, but quite high (~0.5) for P/Q-type channels containing α_{1A} (57) or N-type channels containing α_{1B} (58) as the principle subunit. Previously, we had shown that a chimera containing α_{1C} sequence for its amino-terminal half and α_{1A} sequence for its carboxyl-terminal half had a maximal P_o more like that of α_{1A} than that of α_{1C} (45). The increased P_o for GFP-α_{1S}[III-IVa] compared with GFP-α_{1S} (Fig. 4*C*) now identifies the III-IV loop as an important determinant of P_o. Indeed, our results with GFP-α_{1S}[III-IVa] suggest that the III-IV loop has a quite widespread influence on channel gating. One important goal of future research will be to determine the mechanism whereby the III-IV loop influences the function of L-type channels. For example, do these effects depend only on the interaction of the III-IV loop with proximal portions of the primary sequence (IIIS6, IVS1), or do they depend on interaction of the loop with more distal portions of the primary sequence? Most likely, the interactions are complex because the α_{1S} R1086H mutant displays a hyperpolarizing shift in activation of Ca^{2+} release and a depolarizing shift in activation of L-type Ca^{2+} current (40). In addition to determining the mechanism of III-IV loop effects on L-type channel gating, another important goal for future research will be to determine whether modifying the sequence of the III-IV loop affects gating of N- or P/Q-type channels. It seems possible that the III-IV loop represents a region of hitherto unrecognized importance for the regulation of all the high voltage-activated channels.

Acknowledgments—We thank Drs. N. M. Lorenzon, A. M. Payne, and D. C. Sheridan and J. D. Ohrtman for insightful discussion.

REFERENCES

1. Tanabe, T., Beam, K. G., Powell, J. A., and Numa, S. (1988) *Nature* **336,** 134–139
2. Beam, K. G., and Horowicz, P. (2004) in *Myology* (Engel, A. G., and Franzini-Armstrong, C., eds) pp. 257–280, McGraw Hill, New York
3. Freise, D., Held, B., Wissenbach, U., Pfeifer, A., Trost, C., Himmerkus, N., Schweig, U., Freichel, M., Biel, M., Hofmann, F., Hoth, M., and Flockerzi, V. (2000) *J. Biol. Chem.* **275,** 14476–14481
4. Ursu, D., Sebille, S., Dietze, B., Freise, D., Flockerzi, V., and Melzer, W. (2001) *J. Physiol.* **533,** 367–377
5. Obermair, G. J., Kugler, G., Baumgartner, S., Tuluc, P., Grabner, M., and Flucher, B. E. (2005) *J. Biol. Chem.* **280,** 2229–2237
6. García, K., Nabhani, T., and García, J. (2007) *J. Physiol.* **586,** 727–738
7. Gach, M., Cherednichenko, G., Haarmann, C., Lopez, J. R., Beam, K. G., Pessah, I. N., Franzini-Armstrong, C., and Allen, P. D. (2008) *Biophys. J.* **94,** 3023–3034
8. Beam, K. G., Knudson, C. M., and Powell, J. A. (1986) *Nature* **320,** 168–170
9. Gregg, R. G., Messing, A., Strube, C., Beurg, M., Moss, R., Behan, M., Sukhareva, C., Haynes, S., Powell, J. A., and Coronado, R. (1996) *Proc. Natl. Acad. Sci. U. S. A.* **93,** 13961–13966
10. Tanabe, T., Beam, K. G., Adams, B. A., Niidome, T., and Numa, S. (1990) *Nature* **346,** 567–569
11. Adams, B. A., Tanabe, T., Mikami, A., Numa, S., and Beam, K. G. (1990) *Nature* **346,** 569–572
12. Strube, C., Beurg, M., Sukhareva, C., Ahern, C. A., Powell, J. A., Powers, P. A., Gregg, R. G., and Coronado, R. (1996) *Biophys. J.* **75,** 2531–2543
13. Beurg, M., Ahern, C. A., Vallejo, P., Conklin, M. W., Powers, P. A., Gregg, R. G., and Coronado, R. (1999) *Biophys. J.* **77,** 2953–2967
14. Sheridan, D. C., Carbonneau, L., Ahern, C. A., Nataraj, P., and Coronado, R. (2003) *Biophys. J.* **85,** 3739–3757
15. Sheridan, D. C., Cheng, W., Ahern, C. A., Mortensen, L., Alsammarae, D., Vallejo, P., and Coronado, R. (2003) *Biophys. J.* **84,** 220–237
16. Sheridan, D. C., Cheng, W., Carbonneau, L., Ahern, C. A., and Coronado, R. (2004) *Biophys. J.* **87,** 929–942
17. Schredelseker, J., Di Biase, V., Obermaier, G. J., Felder, E. T., Flucher, B. E., Franzini-Armstrong, C., and Grabner, M. (2005) *Proc. Natl. Acad. Sci. U. S. A.* **102,** 17219–17224
18. Tanabe, T., Mikami, A., Numa, S., and Beam, K. G. (1990) *Nature* **344,** 451–453
19. García, J., Tanabe, T., and Beam, K. G. (1994) *J. Gen. Physiol.* **103,** 125–147
20. Nakai, J., Tanabe, T., Konno, T., Adams, B., and Beam, K. G. (1998) *J. Biol. Chem.* **273,** 24983–24986
21. Kugler, G., Weiss, R. G., Flucher, B. E., and Grabner, M. (2004) *J. Biol. Chem.* **279,** 4721–4728
22. Takekura, H., Paolini, C., Franzini-Armstrong, C., Kugler, G., Grabner, M., and Flucher, B. E. (2004) *Mol. Biol. Cell* **15,** 5408–5419
23. Grabner, M., Dirksen, R. T., Suda, N., and Beam, K. G. (1999) *J. Biol. Chem.* **274,** 21913–21919
24. Wilkens, C. M., Kasielke, N., Flucher, B. E., Beam, K. G., and Grabner, M. (2001) *Proc. Natl. Acad. Sci. U. S. A.* **98,** 5892–5897
25. Bannister, R. A., Papadopoulos, S., and Beam, K. G. (2005) *Biophys. J.* **88,** 640 (abstr.)
26. Ahern, C. A., Bhattacharya, D., Mortensen, L., and Coronado, R. (2001) *Biophys. J.* **81,** 3294–3307
27. Bannister, R. A. (2007) *J. Musc. Res. Cell Motil.* **28,** 275–283
28. Proenza, C., Wilkens, C. M., Lorenzon, N. M., and Beam, K. G. (2000) *J. Biol. Chem.* **275,** 23169–23174
29. Flucher, B. E., Kasielke, N., and Grabner, M. (2000) *J. Cell Biol.* **151,** 467–478
30. Slavik, K. J., Wang, J.-P., Aghdasi, B., Zhang, J.-Z., Mandel, F., Malouf, N., and Hamilton, S. L. (1997) *Am. J. Physiol.* **41,** C1475–C1481
31. Sencer, S., Papineni, R. V., Halling, D. B., Pate, P., Krol, J., Zhang, J. Z., and Hamilton, S. L. (2001) *J. Biol. Chem.* **276,** 38237–38241
32. Papadopoulos, S., Leuranguer, V., Bannister, R. A., and Beam, K. G. (2004) *J. Biol. Chem.* **279,** 44046–44056
33. Lorenzon, N. M., Haarmann, C. S., Norris, E. E., Papadopoulos, S., and Beam, K. G. (2004) *J. Biol. Chem.* **279,** 44057–44064
34. Lorenzon, N. M., and Beam, K. G. (2007) *J. Gen. Physiol.* **130,** 379–388
35. Chen, Y., Li, M., Zhang, Y., He, L., Yamada, Y., Fitzmaurice, A., Shen, Y., Zhang, H., Tong, L., and Yang, J. (2004) *Nature* **429,** 675–680
36. Opatowsky, Y., Chen, C.-C., Campbell, K. P., and Hirsch, J. A. (2004) *Neuron.* **42,** 387–399
37. Van Petegem, F., Clark, K. A., Chatelain, F. C., and Minor, D. L. (2004) *Nature* **429,** 670–675
38. Bannister, R. A., and Beam, K. G. (2005) *Biophys. Biochem. Res. Commun.* **336,** 134–141
39. Monnier, N., Procaccio, V., Stieglitz, P., and Lunardi, J. (1997) *Am. J. Hum. Genet.* **60,** 1316–1325
40. Weiss, R. G., O'Connell, K. M. S., Flucher, B. E., Allen, P. D., Grabner, M., and Dirksen, R. T. (2004) *Am. J. Physiol.* **287,** C1094–C1102
41. Leong, P., and MacLennan, D. H. (1998) *J. Biol. Chem.* **273,** 29958–29964
42. Carbonneau, L., Bhattacharya, D., Sheridan, D. C., and Coronado, R. (2005) *Biophys. J.* **89,** 243–255
43. Beam, K. G., and Franzini-Armstrong, C. (1997) *Methods Cell Biol.* **52,** 283–306
44. Grabner, M., Dirksen, R. T., and Beam, K. G. (1998) *Proc. Natl. Acad. Sci. U. S. A.* **95,** 1903–1908
45. Wilkens, C. M., Grabner, M., and Beam, K. G. (2001) *J. Gen. Physiol.* **118,** 495–508
46. Bannister, R. A., Colecraft, H. M., and Beam, K. G. (2008) *Biophys. J.* **94,** 2631–2638
47. Nakai, J., Dirksen, R. T., Nguyen, H. T., Pessah, I. N., Beam, K. G., and Allen, P. D. (1996) *Nature* **380,** 72–75
48. Avila, G., and Dirksen, R. T. (2000) *J. Gen. Physiol.* **115,** 467–480
49. Avila, G., O'Connell, K. M., Groom, L. A., and Dirksen, R. T. (2001) *J. Biol. Chem.* **276,** 17732–17738
50. Sheridan, D. C., Takekura, H., Franzini-Armstrong, C., Beam, K. G., Allen, P. D., and Perez, C. F. (2006) *Proc. Natl. Acad. Sci. U. S. A.* **103,** 19760–19765
51. Adams, B. A., Mori, Y., Kim, M. S., Tanabe, T., and Beam, K. G. (1994) *J. Gen. Physiol.* **104,** 985–996
52. Adams, B. A., and Beam, K. G. (1989) *J. Gen. Physiol.* **94,** 429–444
53. Sanguinetti, M. C., and Kass, R. S. (1984) *J. Mol. Cell Cardiol.* **16,** 667–670
54. Thomas, G., Chung, M., and Cohen, C. J. (1985) *Circ. Res.* **56,** 87–96
55. Dirksen, R. T., and Beam, K. G. (1995) *J. Gen. Physiol.* **105,** 227–247
56. Cachelin, A. B., de Peyer, J. E., Kokubun, S., and Reuter, H. (1983) *Nature* **304,** 462–464
57. Llinas, R. R., Sugimori, M., and Cherksey, B. (1989) *Ann. N. Y. Acad. Sci.* **560,** 103–111
58. Delcour, A. H., and Tsien, R. W. (1993) *Science.* **259,** 980–984